(Received 12 February 2024, Accepted 27 March 2024, Scheduled 16 April 2024)

Multi-Functional Metamaterial with Polarization and Wide Oblique Angle Insensitivity for X-Band

Punyatoya Routray* and Debalina Ghosh

School of Electrical Science, Indian Institute of Technology Bhubaneswar, India

ABSTRACT: An optimal blend of relatively high frequency and effective atmospheric penetration renders the X-band a versatile selection for a wide range of applications. Hence, metamaterial absorber and frequency selective surface (FSS) as a band-stop filter and shielding element play a significant role in X-band. This article proposes a cost-effective, wide oblique and polarization-insensitive metamaterial, whose applications as an absorber and FSS having band-stop characteristics for X-band are explained. The isotropic unit cell of the proposed metamaterial is designed by an array of two subunit cells, where one is the 90° rotated version of the other with diagonal symmetry. Equivalent circuits of both subunit cells and array structure are systematically designed and analyzed, which provides scope for future modification according to the required frequencies. The proposed absorber provides three absorption peaks and absorptivity of more than 90% up to 60° oblique incidence angle. A good agreement between experimentally measured and simulated results is observed. For the use of the structure as FSS, it has been optimized to provide band-stop characteristics precisely for the X-band up to a wide oblique incidence angle. The proposed design can be used as an absorber, band-stop filter, reflector, and shielding element for the X-band.

1. INTRODUCTION

The rapid advancement of communication technologies has invigorated the quest for materials that can revolutionize signal management and enhance device performance. This has led to the emergence of metamaterials as absorbers, polarizers, and filters used alongside communication devices. Also, the contemporary landscape of warfare systems places an escalating emphasis on low-observable technologies, particularly in the realm of stealth. Metamaterial absorbers are engineered to dissipate incident electromagnetic waves through a combination of conductive and dielectric losses, effectively preventing transmission and reflection [1]. Metamaterial absorbers with their ultra-thin thickness, streamlined fabrication processes, compact size relative to the wavelength, and the capacity for tailoring electromagnetic properties are in preference in comparison to conventional absorbers. On the other hand, Frequency Selective Surfaces (FSSs) are emerging as pivotal elements acting as band-stop filters to reduce interference and crosstalk.

Landy et al.'s report in 2008 introduced the first single-band, polarization-sensitive, and oblique-angle-sensitive metamaterial absorber [2]. Subsequent advancements in this field include the development of single-band and dual-band absorbers featuring petal structures, triple-band absorbers employing a group of dipole structures, and multi-band structures as documented in [3–10]. However, existing multi-band absorbers, as previously reported, exhibit absorption peaks that are widely separated across a broad frequency range. This poses a significant challenge for multi-band operations within a specific frequency band. Single-layered polarization-sensitive metamaterial absorbers and various polarization-independent yet oblique angle-sensitive metamaterial absorbers are presented in [3, 5, 11–14]. While certain single-layered asymmetric metamaterial structures demonstrate impressive absorptivity exceeding 90% over a broad frequency range [15, 16], their utility as metamaterial absorbers is constrained by the presence of high cross-polarization reflection coefficients [16, 17]. Metamaterial absorbers featuring enhanced performance through the incorporation of multiple layers of metal and dielectric, as well as combinations involving gold, graphene, and lumped elements, can be found in [18–22]. However, the drawback of such designs lies in their increased cost and thickness, resulting in intricate structures and inconvenient, time-consuming fabrication processes. In consideration of the need for cost-effectiveness, simplicity, and a convenient fabrication process (one that avoids the use of lumped components or expensive materials like gold and graphene, and steers clear of employing multiple layers of metal and dielectric), this article introduces a single-layered, both polarization and wide oblique angle insensitive metamaterial absorber encompassing all three bands within the X-band frequency range.

The X-band's optimal blend of relatively high frequency and effective atmospheric penetration renders it a versatile selection for a wide array of applications in satellite communication, defense and security, weather monitoring, air traffic control, and numerous other technological domains. As the X-band continues to be a focal point for critical applications, the role of metamaterial absorbers and FSS becomes increasingly significant in addressing interference challenges and advancing the capabilities of communication and radar systems.

* Corresponding author: Punyatoya Routray (pr30@iitbbs.ac.in).

In addition to addressing design considerations, the article also estimates the resonant frequency of a given design and attempts to establish a relationship between its geometry and absorptivity. This article seeks to bridge this gap by offering a thorough exploration of the equivalent circuits for the component subunit cells and the array cells of the metamaterial using a quasi-static approach. This comprehensive approach aims to enhance the theoretical understanding and practical applications of metamaterial absorbers.

The versatility of the structure is demonstrated through its application as a band-stop filter. A metamaterial band-stop filter operates by selectively impeding specific frequencies while allowing others to pass through. These resonant frequencies of the metamaterial correspond to the frequencies targeted for suppression. The band-stop functionality of metamaterials is crucial in scenarios where interference or undesired signals within a specific frequency range need to be mitigated. The proposed design serves as a FSS designed to suppress frequencies within the X-band range.

2. STRUCTURAL DESIGN AND EQUIVALENT CIRCUIT

2.1. Structural Design

Figures 1(a) and 1(b) show the front view of two dual-band metamaterial absorbers, where one is the 90° rotated version of other. They are referred to as subunit cell1 and subunit cell2. Each subunit cell consists of an embedded structure of two sets of rings and split rings and a rod at the center. The objective is to include more resonating elements in a single unit in order to get more absorption peaks. The outer ring and outer split ring form one resonating structure, whereas the second resonating structure is made up of the inner ring, inner split ring, and a centre rod. Both the resonating structures are connected to each other through four metal strips. As lossy substrates are preferred for absorber design, an FR4 substrate of thickness (h) 1 mm, dielectric constant (ϵ_r) of 4, and loss tangent ($\tan\delta$) of 0.02 is chosen as the dielectric layer. The top and bottom metal surfaces are made up of copper having a thickness of 0.035 mm and conductivity of 5.8×10^7 S/m. For practical applications, both metamaterial absorber and FSS as a filter should be insensitive to polarization and oblique incidence. In order to make isotropic structure, the subunit cells are arranged in an array with diagonal symmetry to form a superunit cell. The front view of the proposed superunit cell is shown in Fig. 1(c), where $2w \times 2w$ is the total size. The proposed structure is simulated as an absorber and as FSS using electromagnetic (EM) simulation Computer Simulation Technology (CST) software.

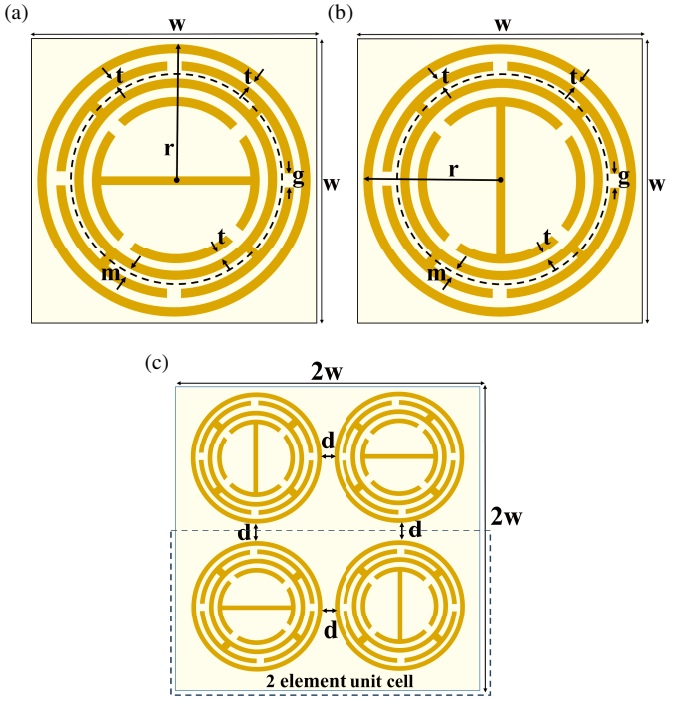

FIGURE 1. Front view of (a) subunit cell1, (b) subunit cell2, (c) proposed super unit cell with geometrical dimension (in mm): $w = 7.2$, $r = 2.89$, $t = 0.2$, $g = 0.4$, $m = 0.14$, $d = 1.42$. The design in the dotted line represents the front view of two element unit cell.

2.2. Equivalent Circuit

For the estimation of resonant frequencies and to get a good perspective of the physics behind the absorptivity related to geometry, the mathematical equivalent circuits are obtained by applying the quasi-static approach. Fig. 2(a) shows equivalent circuits of the subunit cells. The dielectric substrate, separating the top layer and ground plane, is modeled as a section of the transmission line of characteristics impedance Z_T and length h [23, 24]. $Z_T = \frac{Z_0}{\sqrt{\epsilon_r}}$, where Z_0 is the free space impedance, and ϵ_r is the relative dielectric constant of the substrate. The ground plane is treated as a short circuit as it is completely covered with copper.

In the equivalent circuit, L_o is the self-inductance of the outer ring, and C_o is the mutual capacitor between the outer ring and the outer split ring. The outer split ring and inner split ring are represented as a series combination of inductor and capacitance. L_{os}, L_{is} are the inductances of each outer and inner split rings, respectively, and C_g is the capacitance generated due to the splits in the rings.

The inner ring is modeled as series combination of its self-inductance and the mutual capacitance with the outer split ring. To make the equivalent circuit more representable, the inner ring is presented in four parts, i.e., four combinations of L_{i_n} (where $n = 1$ for subunit cell1 and $n = 2$ subunit cell2, respectively) and C_i. The resistances in the equivalent circuit imply the ohmic and other losses related to the surface resistivity of metallization and its surface current density [24–26]. It can be tuned to obtain the absorption level [25]. R_1 and R_2 are the resistances due to the ohmic and other losses in the outer resonating and inner resonating structures, respectively. The outer split ring is connected with the inner ring through four metal strips, which are represented as four short circuits between them in the equivalent circuit.

The lumped elements are calculated by using the standard formulae given below [24, 27–31].

$$L = \frac{\mu N^2 C_1 d_{avg}}{2}\left[\ln\left(\frac{C_2}{\rho}\right) + C_3\rho + C_4\rho^2\right] \quad (1)$$

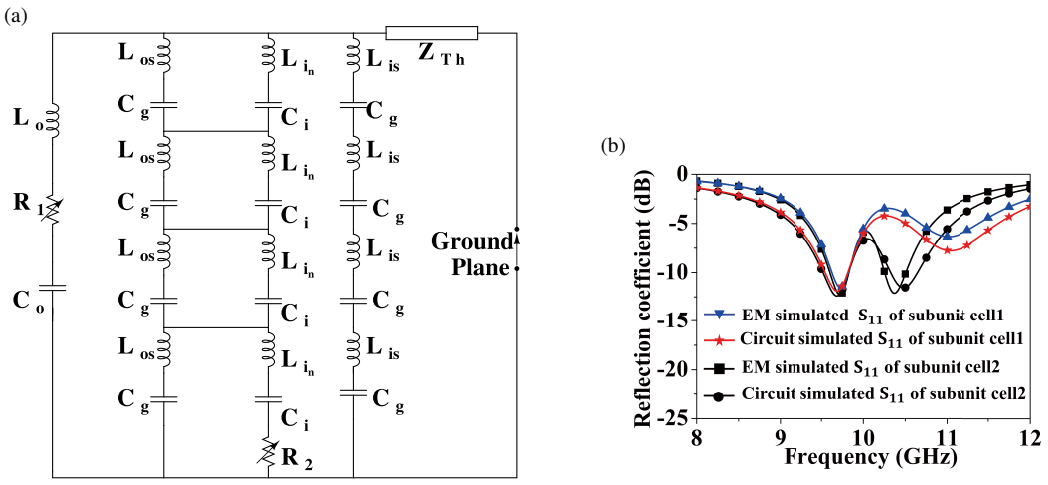

FIGURE 2. (a) Equivalent circuit model. (b) EM simulated and circuit simulated reflection coefficient of both subunit cell1 and subunit cell2.

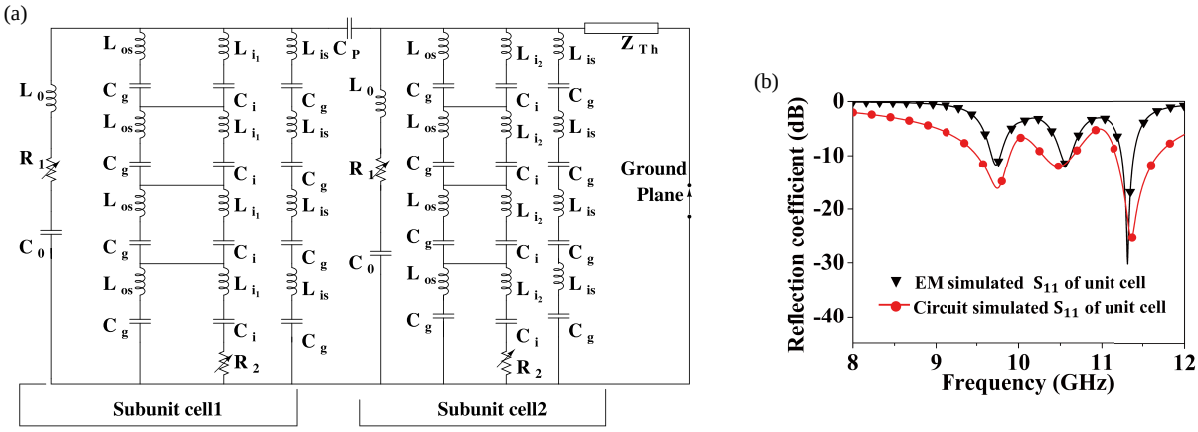

FIGURE 3. (a) Equivalent circuit model of an array of two elements for normally incident EM waves. (b) EM (▼) and circuit (●) simulated reflection coefficient (S_{11}) vs. frequency plots of it.

where

$$d_{avg} = \frac{d_{out} + d_{in}}{2}, \quad \rho = \frac{d_{out} - d_{in}}{d_{out} + d_{in}}$$

$$C_1 = 1, \ C_2 = 2.46, \ C_3 = 0, \ C_4 = 0.20$$

$$L_i = 2\times10^{-4} l \left[\ln\left(\frac{l}{w+t}\right) + 1.193 + 0.2235\left(\frac{w+t}{l}\right)\right] \quad (2)$$

$$C = 2\pi\epsilon_0 \left[\cosh^{-1}\left(\pm\frac{D^2 - {R_1}^2 - {R_2}^2}{2R_1R_2}\right)\right] \quad (3)$$

$$L_s = \mu_0\mu_r h, \quad C_s = \epsilon_0\epsilon_r \frac{h}{2} \quad (4)$$

$$C_g = \frac{\epsilon_o\epsilon_r A}{d} \quad (5)$$

The lumped parameters are calculated using the above formulae, and the equivalent circuit is designed in AWR software. The circuit simulated reflection coefficient plots in AWR software using the lumped parameters of $L_0 = 17.21\,\text{nH}$, $C_0 = 0.01563\,\text{pF}$, $L_{i_1} = 2.945\,\text{nH}$, $L_{i_2} = 3.335\,\text{nH}$, $C_i = 0.07082\,\text{pF}$, $L_{os} = 0.7647\,\text{nH}$, $C_g = 0.000155\,\text{pF}$, $L_{is} = 0.48\,\text{nH}$, $C_s = 0.0177\,\text{pF}$, $L_s = 1.257\,\text{nH}$, $R_1 = 23.2\,\Omega$, $R_2 = 29.8\,\Omega$ closely matches with the EM simulated reflection coefficients (by using CST software), as shown in Fig. 2(b). A slight variation is observed due to inconsideration of mutual capacitance between the inner ring and the inner split ring.

When a metal strip or wire is placed in a time-varying magnetic field and has a orthogonal magnetic component, it produces an electric current, and an inductor is formed [31]. The distributed current in the metal strip at the resonant frequency of 10.4 GHz generates inductance which shifts the resonating frequency to a lower value than subunit cell1. The first resonant frequency is the same as that of subunit cell1 because the outer resonating structure is identical for both.

The mathematical equivalent circuit of an array of two elements is shown in Fig. 3(a). It consists of equivalent circuits of subunit cell1 and subunit cell2 connected through coupling capacitance C_P. C_P is calculated using coupled line theory in [32], and its value is 0.1156 pF. The circuit simulated reflection coefficient of equivalent circuit (shown in Fig. 3(a)) matches with EM simulated results as shown in Fig. 3(b). The

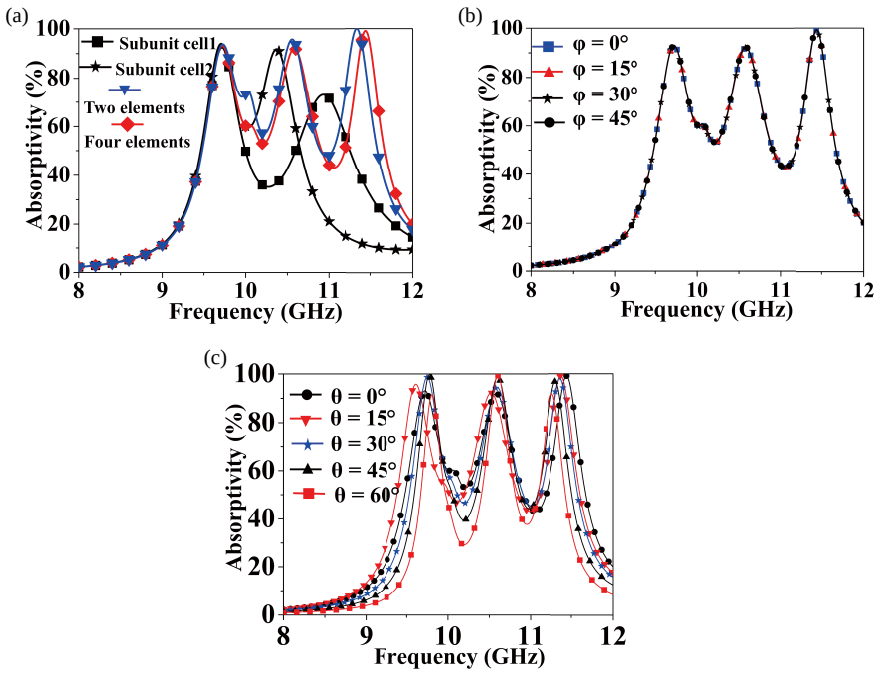

FIGURE 4. (a) Simulated absorptivity of subunit cell1, subunit cell2, two elements unit cell, four elements super unit cell at normal incidence. (b) Simulated absorptivity of proposed absorber different polarization angles and (c) at different oblique incident angles.

equivalent circuit of array of four elements can be obtained by using the same method.

3. METAMATERIAL ABSORBER

3.1. Absorptivity Analysis

Initially, both the subunit cells are designed and simulated using commercially available frequency simulation software. These are excited by a linearly polarized EM wave with the help of periodic boundary condition and Floquet port.

The mathematical formula for the calculation of absorptivity is

$$A = 1 - |R_{xx}|^2 - |R_{xy}|^2 - |T_{xx}|^2 - |T_{xy}|^2 \qquad (6)$$

where R_{xx}, R_{xy} represent co- and cross-polarized reflection coefficients, and T_{xx}, T_{xy} represent co- and cross-polarized transmission coefficients, respectively. The bottom layer of the proposed design is totally covered with copper, which makes both co- and cross-components of the transmission coefficients zero.

The subunit cell1 of the proposed absorber produces two resonating peaks at the frequencies of 9.7 and 10.9 GHz having the absorptivities of 91% and 72%, and subunit cell2 generates two resonating points at 9.7 (same as subunit cell1), and 10.3 GHz with absorptivities of 94% and 92%, respectively, as shown in Fig. 4(a).

In order to obtain more resonating peaks and an increased bandwidth, two subunit cells can be combined to form a unit whose front view is shown in Fig. 1(c) (inside the dotted line). The absorptivity vs. frequency plot in Fig. 4(a) shows three absorptivity peaks at 9.7, 10.5, and 11.3 GHz having the absorptivity of 93%, 92%, and 99%, respectively. But because of asymmetric nature of the structure, the proposed unit cell is polarization sensitive.

In order to make the design polarization insensitive, a superunit is formed taking the combination of subunit cell1 and subunit cell2 with diagonal symmetry as shown in Fig. 1(c). It produces three absorption peaks at frequencies of 9.7, 10.6, and 11.4 GHz with absorptivities of 93%, 92%, and 98%, respectively, as observed from Fig. 4(a). The proposed superunit cell provides a bandwidth of 1.5 GHz from 9.4 to 10.91 GHz and of 0.5 GHz from 11.1 to 11.6 GHz w.r.t full-width at half-maximum (FWHM) value.

To infer the absorptivity w.r.t polarization angles, the designed absorber is simulated by varying polarization angles, and it is observed that the absorptivity of the structure remains unchanged with the variation of polarization angle as shown in Fig. 4(b). Fig. 4(c) presents the absorptivity of the proposed metamaterial with the variation of incident angle, and it is observed that the absorptivities are more than 90% at resonant frequencies and in the same operating band up to 60° oblique incidences.

The influence of geometric parameters such as the width of splits in the rings (g), the radius of the ring (r), and the width of the substrate (w) on the absorptivity of the proposed absorber is investigated. From Fig. 5(a), it can be seen that the resonant frequencies shift towards higher value with increasing 'g'. 'g' is related to the capacitance generated due to splits in the ring, and split capacitance decreases with the increase of width of splits. The inductance value depends on the total current flow path. Hence, the increase of 'r' will increase the current flowing path, which will increase the inductance values and decrease the resonant frequencies as observed from Fig. 5(b). The absorptivity value increases with the increase of 'w' as observed from

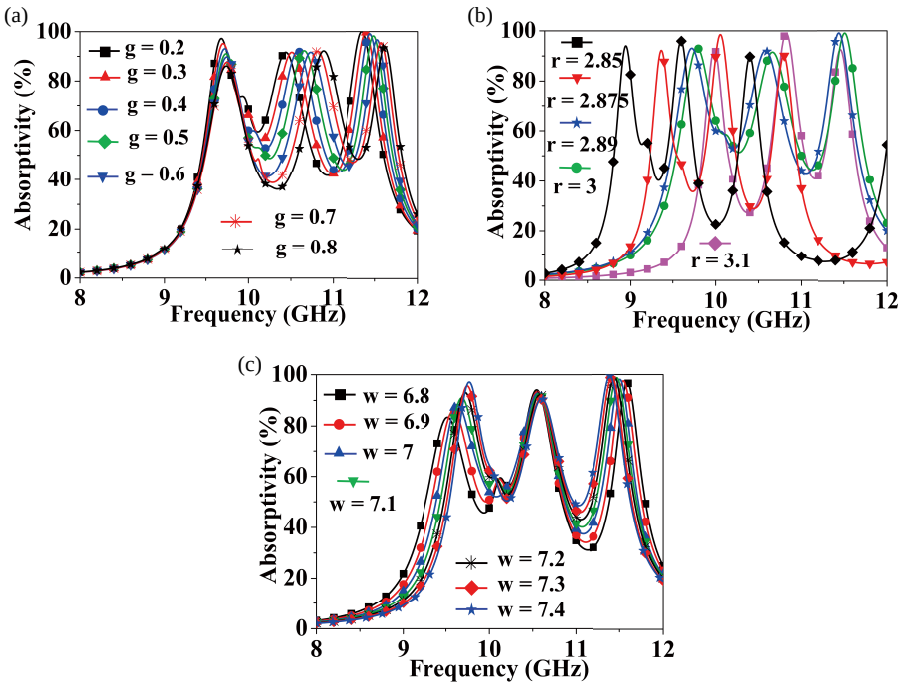

FIGURE 5. (a) Absorptivity plots of proposed absorber with variation of 'g', (b) 'r', (c) 'w'.

Fig. 5(c). Considering both the size of the proposed structure and absorptivity value, the design's width is considered 7.2 mm.

3.2. Absorption Mechanism

Metamaterial absorbers can provide minimum reflection and maximum absorption if their impedance is matched with the free space impedance. To demonstrate the absorption mechanism of a metamaterial by using impedance matching theory, the normalized input impedance of the structure w.r.t free space is calculated using (7)

$$Z = \sqrt{\frac{(1+S_{11})^2 - S_{21}^2}{(1-S_{11})^2 - S_{21}^2}} \tag{7}$$

where S_{11} and S_{21} are extracted from CST. The normalized impedances at the resonant frequencies of 9.7, 10.6, and 11.4 GHz are calculated as follows $Z = 0.7 + \imath 0.1$, $Z = 0.7 + \imath 0.1$, $Z = 1.1 + \imath 0.3$ (Fig. 6). The real and imaginary parts of normalized impedance values are close to 1 and 0, which indicates impedance matching with free space.

The absorption mechanism is also explained by using surface current density plots shown in Fig. 7. From these plots, it is inferred that at the first resonating frequency, the maximum current flows in the outer resonating element of both subcells (Fig. 7(a)). Subunit cell1 is the main contributor to the resonant frequency of 10.6 GHz (Fig. 7(b)), and subunit cell2 is for resonating frequency of 11.4 GHz (Fig. 7(c)).

3.3. Fabrication and Experimental Results

In order to evaluate the performance of the proposed triple-band absorber, the structure is fabricated, and its absorptivity

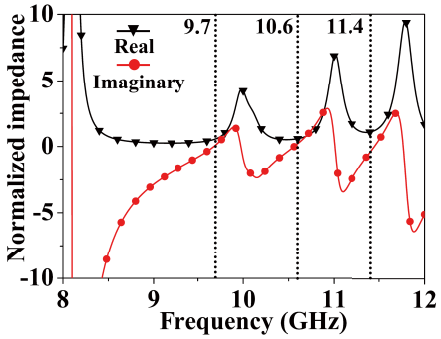

FIGURE 6. Normalised impedance vs. frequency plot showing both real and imaginary part.

is measured under different conditions. A prototype of size 230.4 mm × 230.4 mm is fabricated on a planer sheet of FR4 substrate (thickness 1 mm) using standard printed circuit board (PCB) technology. The whole structure with its enlarged portion is shown in Fig. 8(a). The experimental setup shown in Fig. 8(b) consists of a Rhode and Schwarz ZVA 24 vector network analyzer with a frequency range of 10 MHz to 24 GHz. Two linearly polarized horn antennas of model UWB-5148 with dimensions 27.9 × 31 × 22.7 cm^3 operating between 0.8 and 18 GHz with a minimum gain of 7 dBi and a maximum gain of 14 dBi are used as transmitting and receiving antennas. The fabricated prototype is kept at a distance of 3 m in front of the antennas to satisfy the far-field conditions.

Initially, the reflection coefficient of the fabricated absorber is measured. Then, it is replaced with a copper plate of the same dimension, and again, the reflection coefficient is measured. The difference between the reflection coefficient of the fabricated absorber and the copper plate is the actual reflection

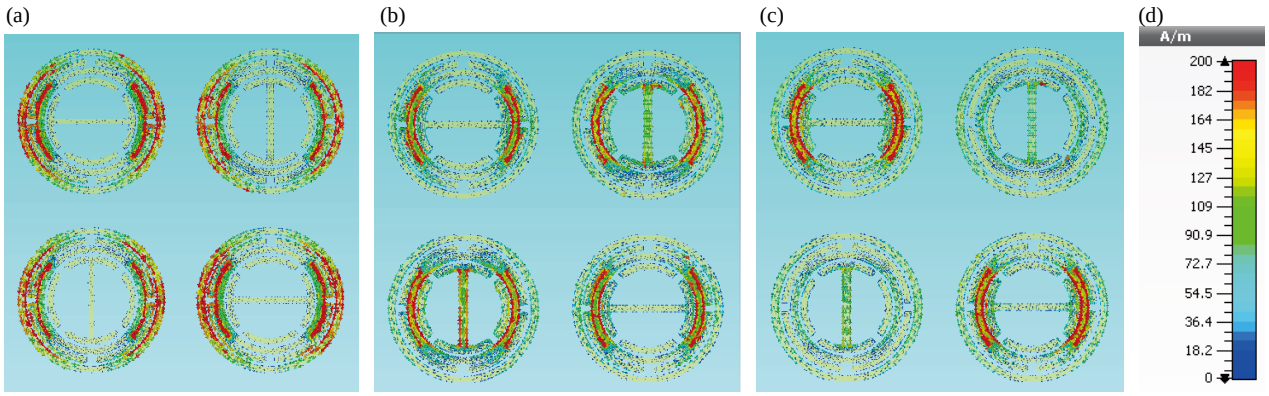

FIGURE 7. Surface current density in the top layer at frequencies of (a) 9.7 GHz, (b) 10.6 GHz, (c) 11.4 GHz.

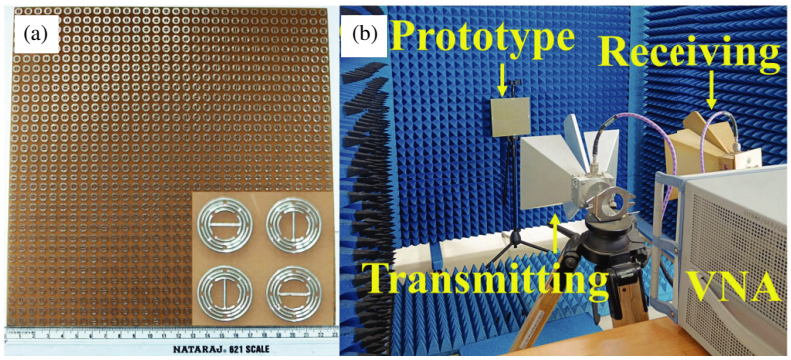

FIGURE 8. (a) Experimental prototype with its enlarged view of the unit cell, (b) experimental set up for measurement.

coefficient for the measurement of the absorptivity. During the measurement, environmental imperfections such as diffraction loss, scattering loss, and other signals will be canceled out as the fabricated absorber and copper plate are illuminated in identical surroundings.

Figure 9(a) shows a comparison of experimentally measured and simulated absorptivity plots. It shows three resonating peaks at the frequencies of 9.7, 10.5, and 11.4 GHz with the absorptivities of 98%, 97%, and 96%, respectively and also provides a bandwidth same as simulated one. In order to inspect the polarization behavior of the proposed absorber in real-world environment, the absorptivity of the proposed design is measured w.r.t the polarization angle. The position and orientation of both the transmitting and receiving antennas are kept constant, and the fabricated structure is rotated from $0°$ to $45°$. The same procedures of measurement of absorptivity at normal incidence are repeated. The measured absorptivity vs. frequency plot for different polarization angles (Fig. 9(b)) depicts similar behavior, demonstrating polarization-insensitive nature of the absorber.

Next, the absorber is kept in a fixed position while both the transmitting and receiving antennas are rotated through a common angle for the analysis of absorptivity at varying of oblique angles. The absorptivity vs. frequency plots at different oblique angles (Fig. 4(a) and Fig. 9(c)) show a good agreement between the measured and simulated results.

3.4. Comparison Table

Table 1 presents a comparative analysis of the performance of the proposed structure as an absorber in comparison to the metamaterial absorbers already documented in the literature.

The determination of the number of bands is based on the identification of absorption peaks that have an absorptivity above 90%. The stability of an oblique angle is determined by the angle up to which the absorptivity exceeds 90% at the resonant frequencies.

The comparison table shows that the proposed absorber provides all three absorption peaks in the X band with $60°$ oblique angle stability. An equivalent circuit is modeled in order to get an idea for future modifications according to required frequencies.

4. FILTER USING FSS

Frequency selective surfaces are the periodic arrangement of similar elements having a wide range of applications, such as spatial filters, antenna reflectors, electromagnetic band gap materials, and absorbers. FSS as filters are the appropriate replacement for conventional filters because of their smaller size, easy fabrication process, flexible and multipurpose functionality [36]. For the application of the structure (Fig. 1) as a band-stop filter, the ground plane of the design is removed, and the geometrical parameters are optimized to $w = 7.22$, $r = 3.6$,

TABLE 1. Comparison of the proposed absorber with previously presented absorbers.

Ref.	No of bands	Frequency bands	Oblique angle stability	Equivalent circuit analysis
[33]	2	X	30°	No
[4]	2	K	60°	No
[29]	3	C, X	45°	Yes
[34]	3	X, Ku, K	X	Yes
[35]	4	S, X, Ku	45°	No
[10]	3	C, X, Ku	60°	Yes
This work	3	X	60°	Yes

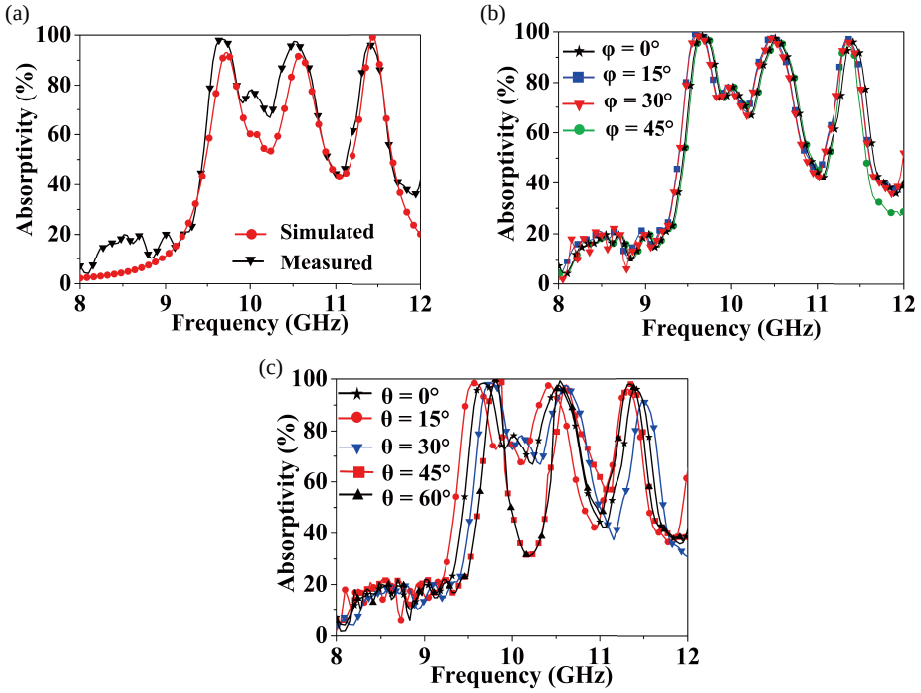

FIGURE 9. Measured absorptivity of proposed absorber at (a) normal incidence, (b) different polarization angles, (c) different oblique incident angles.

$t = 0.2$, $g = 0.4$, $m = 1$, $d = 0.04$ (mm). S-parameters of the subunit cells and quadrature unit cell are plotted as a function of frequency at normal incidence for both TE and TM polarized EM waves in Figs. 10(a) and 10(b), respectively. Subunit cell1 and subunit cell2 shown in Figs. 1(a) and 1(b) provide two resonant frequencies for both TE and TM modes as they contain two resonating structures (Fig. 10(a)). Their responses are different w.r.t TE and TM modes, making the structures polarization sensitive, as shown in Fig. 10(a).

The proposed FSS (Fig. 1(c)) is mainly designed for X-band application, which suppresses the frequency precisely from 8 to 12 GHz with a minimum −10 dB insertion loss (Fig. 10(b)). Within this frequency range, the reflection coefficient remains close to 0 dB, as depicted in Fig. 10(b). The frequency responses are similar for both TE and TM modes. The transmission coefficient of the proposed FSS is plotted w.r.t polarization angles for both TE and TM modes in Figs. 11(a) and 11(b). The response is consistent across all the polarization angles, demonstrating the polarization-insensitive behavior.

The transmission responses of the quadrature FSS at different oblique incidence angles for both TE and TM modes are shown in Figs. 12(a) and 12(b). In TE mode, the resonance frequency in the X-band shifts slightly, and the bandwidth w.r.t −10 dB increases as the oblique angle increases. However, in TM mode, the bandwidth and resonant frequency in the X-band remain constant up to an oblique incidence angle of 45° with only slight changes at 60°.

4.1. Parametric Analysis

In Fig. 13, the transmission coefficient of the proposed design is plotted at different loss tangent values, and it is observed that for lossless substrate, the design provides two passbands at frequencies of 6.1 and 12 GHz with a transmission coefficient close to 0 dB. For this lossless condition, the transmission coefficient values at resonant frequencies are minimal, and these increase with the increased loss without affecting bandwidth.

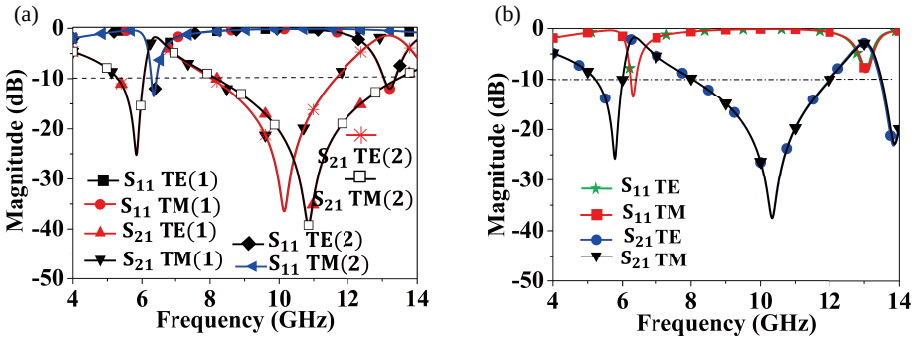

FIGURE 10. (a) Plot of S parameters at normal incidence for TE and TM modes of subunit cells where 1 denotes subunit cell1 and 2 subunit cell2. (b) Plot of S parameters at normal incidence for TE and TM modse of proposed FSS.

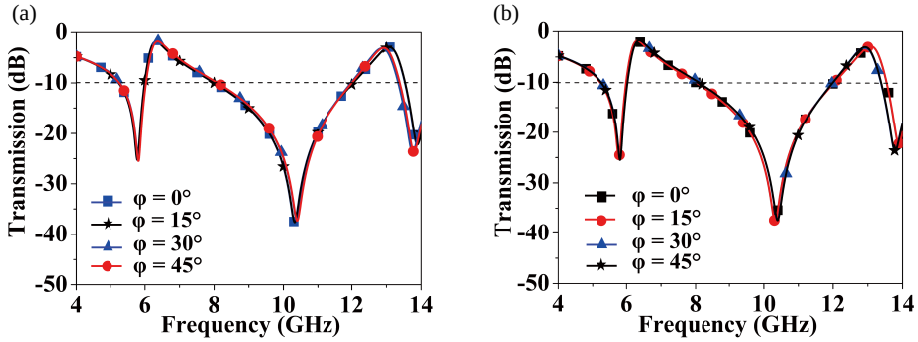

FIGURE 11. Transmission coefficient vs. frequency plot of proposed FSS at different polarization angles for (a) TE mode, (b) TM modes.

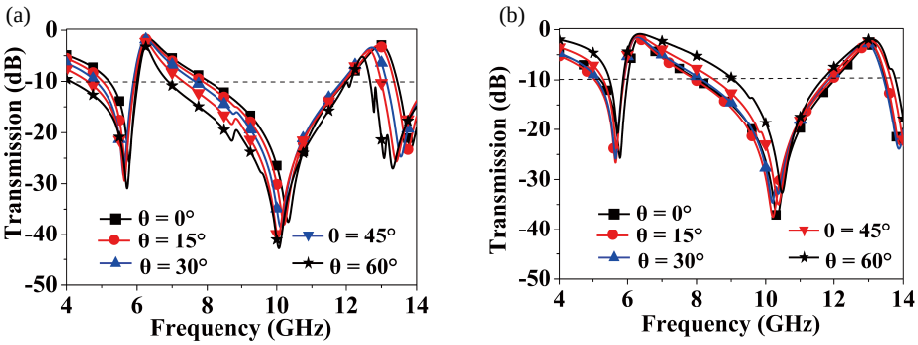

FIGURE 12. Transmission coefficient vs. frequency plot of proposed FSS at different oblique angles for (a) TE mode, (b) TM modes.

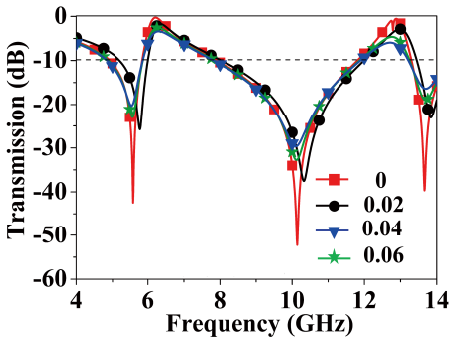

FIGURE 13. Transmission coefficient vs. frequency plot of proposed FSS at different substrate loss ($\tan\delta$) with the enlarged view of response for lossless condition.

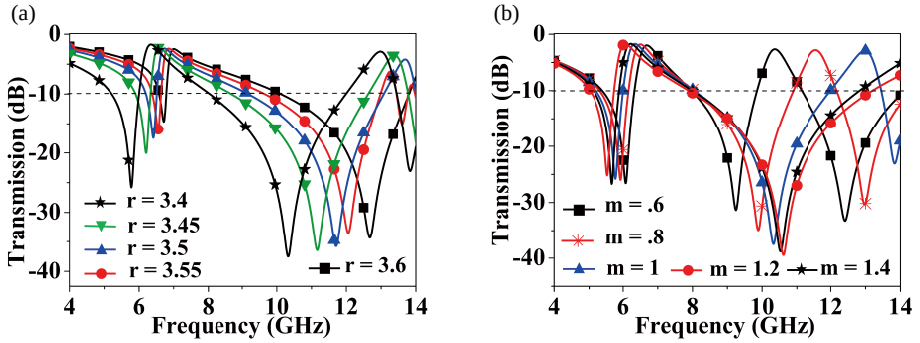

FIGURE 14. Transmission coefficient vs. frequency plot of proposed FSS at different value of (a) 'r', i.e., the radious of outer ring, (b) 'm', i.e., the separation between outer and inner resonating structure.

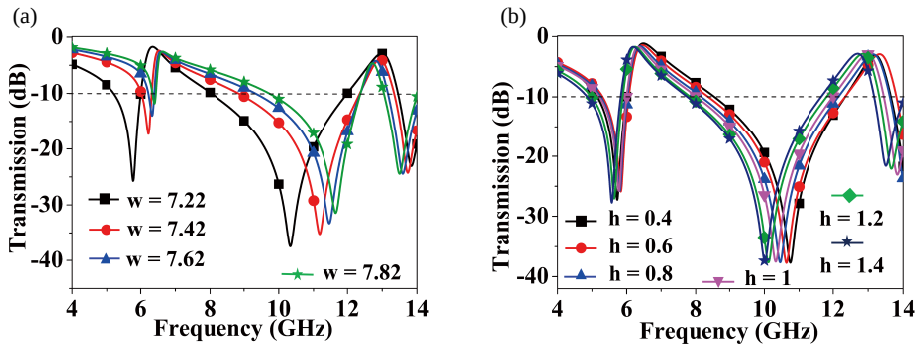

FIGURE 15. Transmission coefficient vs. frequency plot of proposed FSS at different value of (a) 'w', i.e., $2 \times w$ is the width of the substrate, (b) 'h', i.e., the thickness of the substrate.

The transmission coefficient is plotted at different 'r' and 'm' values in Figs. 14(a) and 14(b), where 'r' is the radius of the outer ring, and 'm' is the separation between the outer and inner resonating structures. The variation in 'r' changes the size of all resonating elements, while the variation in 'm' only changes the size of the inner resonating structure, keeping the size of the outer resonating structure constant. From Fig. 14(a), it is seen that the resonating points shift to a lower value with an increase of 'r', and at 'r' $= 3.6$, it suppresses the exact X-band frequency. The rise in 'm' moves the second resonating point to a higher frequency, keeping the first resonating point almost constant; as a result, bandwidth increases with the increase of 'm', as shown in Fig. 14(b).

The coupling between the elements decreases with the increase of 'w' ($2 \times w$ is the width of the substrate); as a result, bandwidth decreases, as depicted in Fig. 15(a). The bandwidth is almost constant with the variation of the thickness of the substrate 'h' (Fig. 15(b)), and the resonant frequency in the X-band shifts slightly to a lower value with an increase of 'h'.

5. CONCLUSION

A cost-effective, wide oblique and polarization angle insensitive metamaterial absorber having all three bands in the X-band frequency range is proposed in this article. The equivalent circuits are modeled for both subunit cells and an array of two element unit cell, which gives an idea for future modifications according to the required frequency. The proposed design is fabricated using a low-cost FR4 substrate through an inexpensive PCB fabrication process, and a good agreement between the measured and simulated results is obtained. Further, the design with optimized dimension can be used as a filter which suppresses the X-band frequency range to reduce the interference. The FSS provides an insensitive band-stop response to both TE and TM modes and a stable response for wide oblique incidence angle in the X-band. The structure can also be used as a reflector and shielding element.

REFERENCES

[1] Engheta, N. and R. W. Ziolkowski, *Metamaterials: Physics and Engineering Explorations*, John Wiley & Sons, 2006.

[2] Landy, N. I., S. Sajuyigbe, J. J. Mock, D. R. Smith, and W. J. Padilla, "Perfect metamaterial absorber," *Physical Review Letters*, Vol. 100, No. 20, 207402, 2008.

[3] Costa, F., S. Genovesi, A. Monorchio, and G. Manara, "A circuit-based model for the interpretation of perfect metamaterial absorbers," *IEEE Transactions on Antennas and Propagation*, Vol. 61, No. 3, 1201–1209, 2012.

[4] Wang, J., R. Yang, J. Tian, X. Chen, and W. Zhang, "A dual-band absorber with wide-angle and polarization insensitivity," *IEEE Antennas and Wireless Propagation Letters*, Vol. 17, No. 7, 1242–1246, 2018.

[5] Zhai, H., C. Zhan, Z. Li, and C. Liang, "A triple-band ultrathin metamaterial absorber with wide-angle and polarization stability," *IEEE Antennas and Wireless Propagation Letters*, Vol. 14, 241–244, 2014.

[6] Binda, P., R. K. Singh, and R. Mitharwal, "An ultra-thin, polarization free wide-angle stable quad-band metamaterial absorber for applications in C, X, and Ku bands," *AEU — International Journal of Electronics and Communications*, Vol. 171, 154925, 2023.

[7] Routray, P. and D. Ghosh, "Wide oblique incidence insensitive ultra-thin dual-band metamaterial absorber," in *2023 International Conference on Microwave, Optical, and Communication Engineering (ICMOCE)*, 1–5, 2023.

[8] Wu, T., Y.-M. Ma, J. Chen, and L.-L. Wang, "A low profile quadruple-band polarization insensitive metamaterial absorber," *Progress In Electromagnetics Research M*, Vol. 90, 69–79, 2020.

[9] Bathani, N. J. and J. Rathod, "Analysis of conformal quad band metamaterial absorber design on planar and cylindrical surface," *Progress In Electromagnetics Research M*, Vol. 103, 37–47, 2021.

[10] Routray, P. and D. Ghosh, "Design and modeling of a miniaturized multi-layer metamaterial absorber with oblique angle and polarization insensitivity," *IEEE Letters on Electromagnetic Compatibility Practice and Applications*, Vol. 6, No. 1, 29–34, 2024.

[11] Jiang, Z. H., S. Yun, F. Toor, D. H. Werner, and T. S. Mayer, "Conformal dual-band near-perfectly absorbing mid-infrared metamaterial coating," *ACS Nano*, Vol. 5, No. 6, 4641–4647, 2011.

[12] Tao, H., C. M. Bingham, A. C. Strikwerda, D. Pilon, D. Shrekenhamer, N. I. Landy, K. Fan, X. Zhang, W. J. Padilla, and R. D. Averitt, "Highly flexible wide angle of incidence terahertz metamaterial absorber: Design, fabrication, and characterization," *Physical Review B*, Vol. 78, No. 24, 241103, 2008.

[13] Zuo, W., Y. Yang, X. He, D. Zhan, and Q. Zhang, "A miniaturized metamaterial absorber for ultrahigh-frequency RFID system," *IEEE Antennas and Wireless Propagation Letters*, Vol. 16, 329–332, 2016.

[14] Routray, P. and D. Ghosh, "Quadruple polarization insensitive multilayered metamaterial absorber," in *2022 IEEE Wireless Antenna and Microwave Symposium (WAMS)*, 1–4, IEEE, 2022.

[15] Ghosh, S., S. Bhattacharyya, D. Chaurasiya, and K. V. Srivastava, "An ultrawideband ultrathin metamaterial absorber based on circular split rings," *IEEE Antennas and Wireless Propagation Letters*, Vol. 14, 1172–1175, 2015.

[16] Routray, P. and D. Ghosh, "Analysis of a wideband hybrid metamaterial as an absorber vis-a-vis a polarizer," in *2022 IEEE Microwaves, Antennas, and Propagation Conference (MAPCON)*, 101–105, IEEE, 2022.

[17] Ahmed, F., T. Hassan, and N. Shoaib, "Comments on "An ultrawideband ultrathin metamaterial absorber based on circular split rings"," *IEEE Antennas and Wireless Propagation Letters*, Vol. 19, No. 3, 512–514, 2020.

[18] Rajyalakshmi, G., Y. R. Kumar, D. Ramakrishna, and K. S. Rao, "Angle independent metamaterial absorber for S and C band application," *Progress In Electromagnetics Research C*, Vol. 130, 241–254, 2023.

[19] Pan, W., X. Yu, J. Zhang, and W. Zeng, "A novel design of broadband terahertz metamaterial absorber based on nested circle rings," *IEEE Photonics Technology Letters*, Vol. 28, No. 21, 2335–2338, 2016.

[20] Qi, L. and C. Liu, "Broadband multilayer graphene metamaterial absorbers," *Optical Materials Express*, Vol. 9, No. 3, 1298–1309, 2019.

[21] Zuo, W., Y. Yang, X. He, C. Mao, and T. Liu, "An ultrawideband miniaturized metamaterial absorber in the ultrahigh-frequency range," *IEEE Antennas and Wireless Propagation Letters*, Vol. 16, 928–931, 2016.

[22] Shi, T., L. Jin, L. Han, M.-C. Tang, H.-X. Xu, and C.-W. Qiu, "Dispersion-engineered, broadband, wide-angle, polarization-independent microwave metamaterial absorber," *IEEE Transactions on Antennas and Propagation*, Vol. 69, No. 1, 229–238, 2020.

[23] Li, S.-J., X.-Y. Cao, J. Gao, T. Liu, Y.-J. Zheng, and Z. Zhang, "Analysis and design of three-layer perfect metamaterial-inspired absorber based on double split-serration-rings structure," *IEEE Transactions on Antennas and Propagation*, Vol. 63, No. 11, 5155–5160, 2015.

[24] Ebrahimi, A., S. Nirantar, W. Withayachumnankul, M. Bhaskaran, S. Sriram, S. F. Al-Sarawi, and D. Abbott, "Second-order terahertz bandpass frequency selective surface with miniaturized elements," *IEEE Transactions on Terahertz Science and Technology*, Vol. 5, No. 5, 761–769, 2015.

[25] Bhattacharyya, S., S. Ghosh, and K. V. Srivastava, "Equivalent circuit model of an ultra-thin polarization-independent triple band metamaterial absorber," *AIP Advances*, Vol. 4, No. 9, 097127, 2014.

[26] Moallem, M. and K. Sarabandi, "Miniaturized-element frequency selective surfaces for millimeter-wave to terahertz applications," *IEEE Transactions on Terahertz Science and Technology*, Vol. 2, No. 3, 333–339, 2012.

[27] Rosa, E. B. and F. W. Grover, "Formulas and tables for the calculation of mutual and self-inductance," *Journal of the Washington Academy of Sciences*, Vol. 1, No. 1/2, 14–16, 1911.

[28] Kurra, L., M. P. Abegaonkar, and S. K. Koul, "Equivalent circuit model of resonant-EBG bandstop filter," *IETE Journal of Research*, Vol. 62, No. 1, 17–26, 2016.

[29] Singh, A. K., M. P. Abegaonkar, and S. K. Koul, "Dual- and triple-band polarization insensitive ultrathin conformal metamaterial absorbers with wide angular stability," *IEEE Transactions on Electromagnetic Compatibility*, Vol. 61, No. 3, 878–886, 2018.

[30] Smythe, W. B., *Static and Dynamic Electricity*, Hemisphere Publishing, New York, NY (USA), 1988.

[31] Bayatpur, F., "Metamaterial-inspired frequency-selective surfaces," Ph.D. dissertation, University of Michigan, 2009.

[32] Ghosh, S. and K. V. Srivastava, "An equivalent circuit model of FSS-based metamaterial absorber using coupled line theory," *IEEE Antennas and Wireless Propagation Letters*, Vol. 14, 511–514, 2014.

[33] Tak, J. and J. Choi, "A wearable metamaterial microwave absorber," *IEEE Antennas and Wireless Propagation Letters*, Vol. 16, 784–787, 2016.

[34] Hannan, S., M. T. Islam, N. M. Sahar, K. Mat, M. E. H. Chowdhury, and H. Rmili, "Modified-segmented split-ring based polarization and angle-insensitive multi-band metamaterial absorber for X, Ku and K band applications," *IEEE Access*, Vol. 8, 144 051–144 063, 2020.

[35] Singh, R. K. and A. Gupta, "A wrenched-square shaped polarization independent and wide angle stable ultra-thin metamaterial absorber for S-band, X-band and Ku-band applications," *AEU — International Journal of Electronics and Communications*, Vol. 132, 153648, 2021.

[36] Bashiri, M., C. Ghobadi, J. Nourinia, and M. Majidzadeh, "WiMAX, WLAN, and X-band filtering mechanism: Simple-structured triple-band frequency selective surface," *IEEE Antennas and Wireless Propagation Letters*, Vol. 16, 3245–3248, 2017.